CellPress
OPEN ACCESS

Supplemental figures

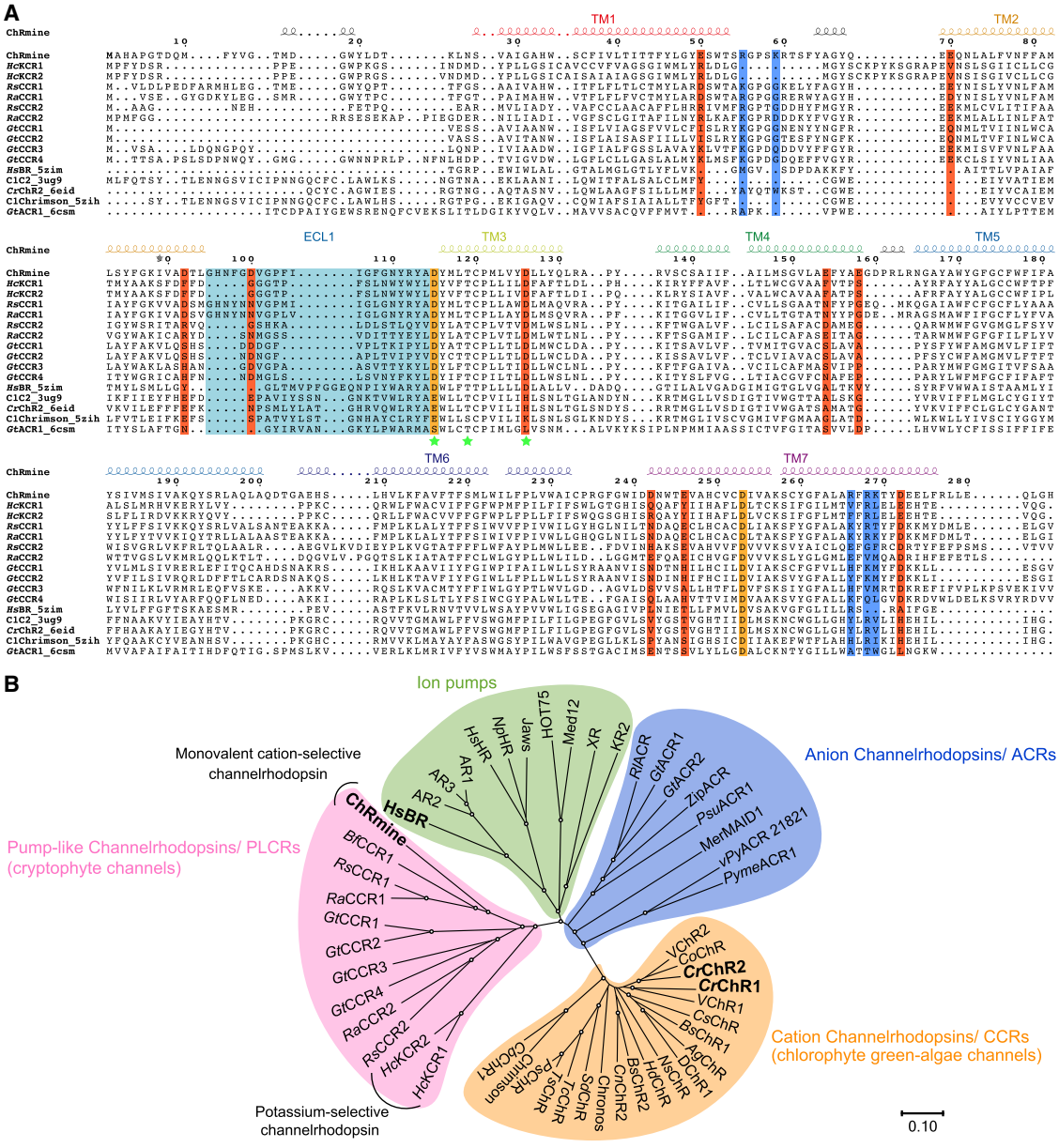

(legend on next page)

Figure S1. Structure-based sequence alignment, phylogenetic tree, and predicted structure of ChRmine, related to Figure 1

(A) The sequences are ChRmine (GenBank: QDS02893.1), *Hc*KCR1 (GenBank: MZ826862) (Govorunova et al., 2021), *Hc*KCR2 (GenBank: MZ826861) (Govorunova et al., 2021), *Ra*CCR1 (GenBank: QIU80793.1), *Rs*CCR1 (GenBank: QIU80800.1), *Ra*CCR2 (GenBank: QIU80796.1), *Rs*CCR2 (GenBank: QIU80801.1), *Gt*CCR1 (GenBank: ANC73520.1), *Gt*CCR2 (GenBank: ANC73518.1), *Gt*CCR3 (GenBank: ANC73519.1), *Gt*CCR4 (GenBank: ARQ20888.1), *Hs*BR (PDB: 5ZIM) (Hasegawa et al., 2018), C1C2 (PDB: 3UG9) (Kato et al., 2012), *Cr*ChR2 (PDB: 6EID) (Volkov et al., 2017), C1Chrimson (PDB: 5ZIH) (Oda et al., 2018), *Gt*ACR1 (PDB: 6CSM) (Kim et al., 2018), *Cr*ChR1 (GenBank: AAL08946.1), VChR1 (GenBank: ABZ90900.1), VChR2 (GenBank: ABZ90902.1), Chronos (GenBank: KF992040.1), *Gt*ACR2 (GenBank: AKN63095.1), *Rl*ACR (GenBank: APZ76712.1), MerMAID1 (GenBank: QCW06519.1) (Oppermann et al., 2019), *Pyme*ACR1 (GenBank: QNU12853.1) (Rozenberg et al., 2020), v*Py*ACR_21821 (GenBank: QNU12854.1) (Rozenberg et al., 2020), *Hs*HR (PDB: 1E12) (Kolbe et al., 2000), *Med12*BPR (PDB: 4JQ6) (Ran et al., 2013), XR (PDB: 3DDL) (Luecke et al., 2008), and KR2 (PDB: 3X3B) (Kato et al., 2015b). The sequence alignment was created using PLOMALS3D (Pei et al., 2008) and ESPript 3 (Robert and Gouet, 2014) servers. Secondary structure elements for ChRmine are shown as coils. Positively and negatively charged residues are highlighted in blue and red, respectively. Green stars represent the DTD motif. The ECL1 of ChRmine is colored light blue. The counterions are colored orange.

(B) An unrooted phylogenetic tree was drawn for representative microbial rhodopsins using the neighbor-joining method (Saitou and Nei, 1987), and 1,000 bootstrap replicates. Evolutionary analyses were conducted in MEGA7 (Kumar et al., 2016). White circles represent bootstrap values >85%.

(C–F) Five predicted models of ChRmine, generated using locally installed AlphaFold2. The ribbon representations are colored by the pLDDT score (low, red; high, cyan).

(C) Plots of the pLDDT score.

(D) The best predicted model superimposed onto the cryo-EM structure (yellow).

(E and F) The detailed comparison of ECL1 (E) and the Schiff base region (F) between the five predicted models and cryo-EM structure. Notably, the C-terminal region of ECL1, including D115, has high pLDDT scores, but the conformation of D115 is not correctly predicted.

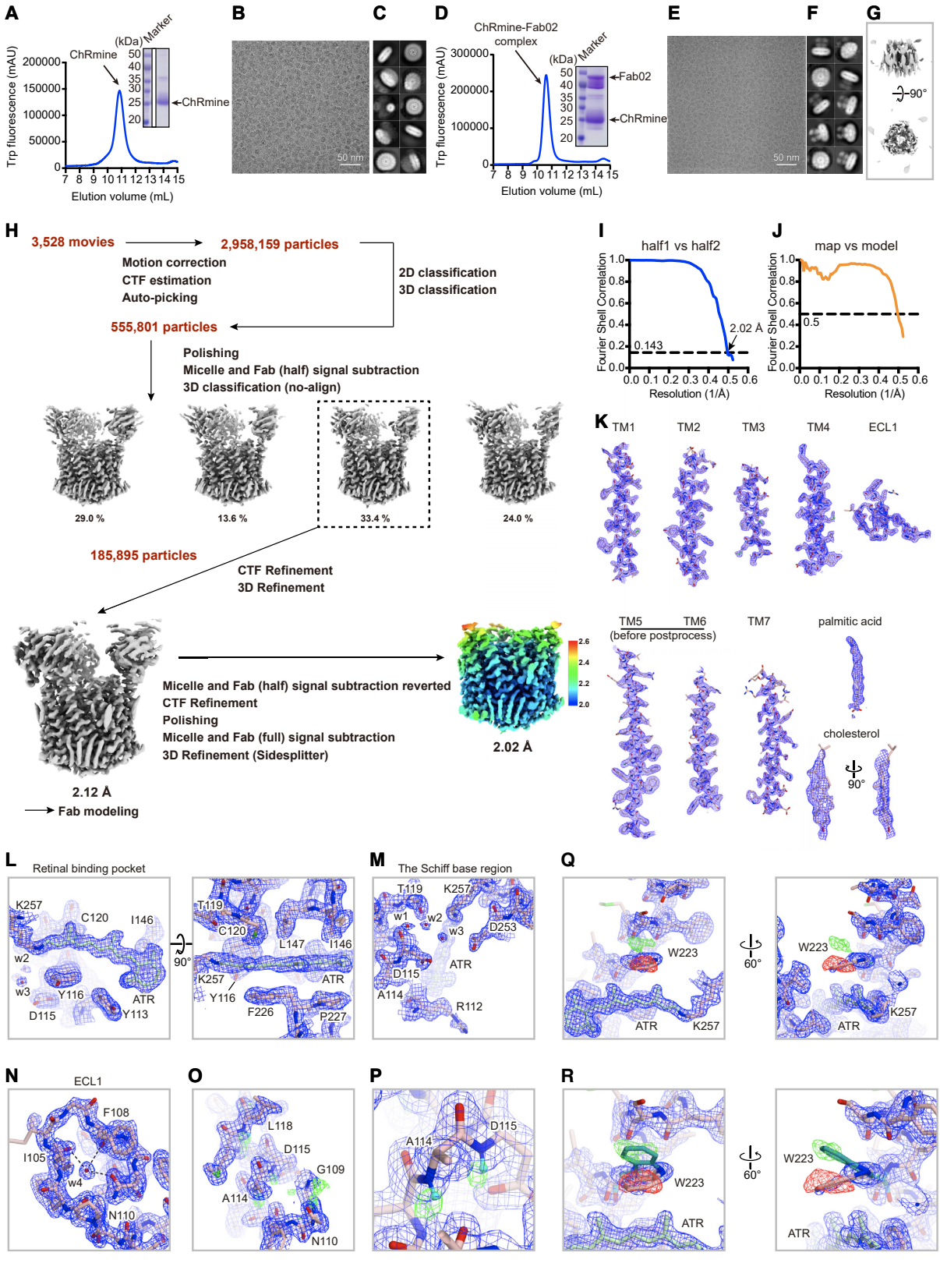

(legend on next page)

Figure S2. Cryo-EM analysis of the ChRmine and ChRmine-Fab02 complex, related to Figure 1

(A–C) Panels corresponding to ChRmine alone. Representative SEC trace with SDS-PAGE as inset (A), representative cryo-EM micrograph (B), and 2D-class averages (C).

(D–F) Panels corresponding to the ChRmine-Fab02 complex. Representative SEC trace with SDS-PAGE as inset (D), representative cryo-EM micrograph (E), and 2D-class averages (F).

(G) Low-resolution reconstruction of ChRmine alone.

(H) Data processing workflow of the ChRmine-Fab02 complex. Final cryo-EM map colored by local resolution.

(I) Fourier shell correlation (FSC) between the two independently refined half-maps.

(J) FSC between the model and the map calculated for the model refined against the full reconstruction.

(K–N) Cryo-EM density (FSC-weighted sharpened map calculated by RELION3.1.1) and model for ChRmine, lipids (K), the retinal binding pocket (L), the Schiff base region (M), and twisted ECL1 (N).

(O and P) Density and model near ECL1 region. FSC-weighted sharpened map calculated by RELION3.1.1 (blue) and F_o-F_c map calculated by Servalcat (green). Positive F_o-F_c difference densities (4.3σ, where σ is the standard deviation within the mask) are observed near nitrogen atoms, suggesting that these densities represent hydrogen atoms.

(Q and R) Possible signal of early photo-intermediate. (Q) Density and model in the retinal binding pocket region. Blue and green maps are FSC-weighted sharpened map calculated by RELION3.1.1 and F_o-F_c maps calculated by Servalcat, respectively. Positive and negative F_o-F_c difference density pairing ($\pm$3.7σ, where σ is the standard deviation within the mask) is observed around W223, suggesting that this density contains information regarding a small population of the early intermediate state, and that W223 moves upward early in the photocycle. (R) Magnified views of (Q).

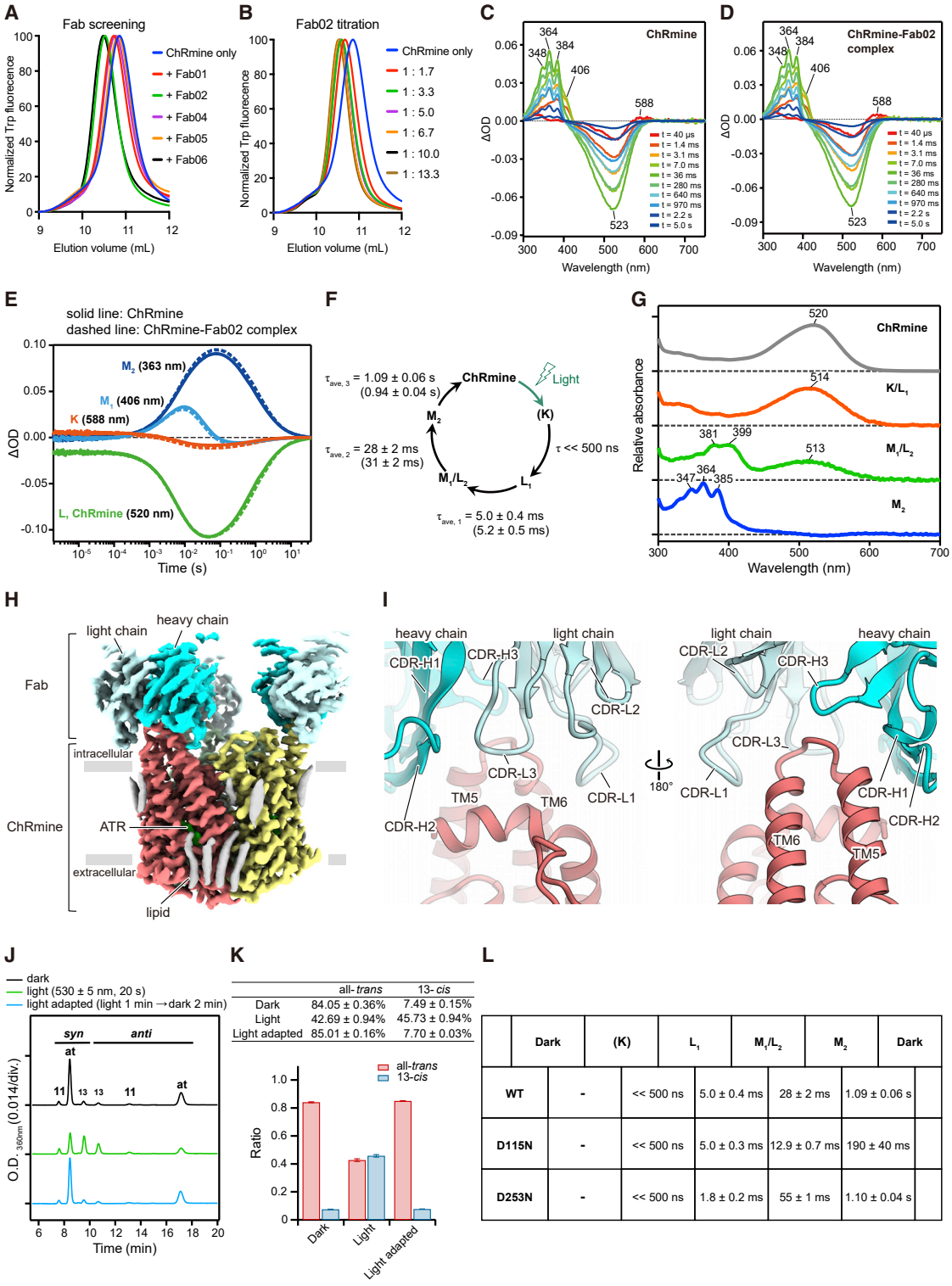

Figure S3. Spectroscopic, structural, and HPLC characterization of the ChRmine and ChRmine-Fab02 complex, related to Figure 1

(A) FSEC screening of Fab fragments.

(B) Titration of the Fab02 fragment against ChRmine.

(C and D) Transient absorption spectra of ChRmine WT (C) and the ChRmine-Fab02 complex (D) excited at λ_{exc} = 532 nm.

(legend continued on next page)

(E) Time-series traces of absorption changes of ChRmine WT (solid line) and the ChRmine-Fab02 complex (dashed line) at 363 (blue), 406 (cyan), 520 (green), and 588 nm (red) probe wavelengths.
(F) Photocycle scheme of ChRmine determined by flash photolysis shown in (E). The lifetimes of ChRmine-Fab02 are shown in parentheses.
(G) The absorption spectra of the initial state (gray), L_1 (orange), M_1/L_2 (green), and M_2 (blue) of ChRmine calculated from the decay-associated spectra of transient absorption changes (Inoue et al., 2013).
(H) Cryo-EM map of the ChRmine-Fab02 complex.
(I) Interactions between ChRmine and Fab02.
(J and K) HPLC analysis of the chromophore configuration of ChRmine. (J) Representative HPLC profiles of the chromophore of ChRmine in the dark (top), under illumination (middle), and after light adaptation (bottom). "At," "11," and "13" indicate the peak of all-*trans*-, 11-*cis*-, and 13-*cis*-retinal oximes, respectively. (K) Calculated composition of all-*trans*- and 13-*cis*-retinal oximes. Data are presented as mean ± SEM (n = 3). Purified samples of ChRmine were prepared with additional supplementation of all-*trans* retinal. Green light (530 ± 5 nm) was used for illumination. Light adaptation was achieved by illumination for 1 min followed by incubation in the dark for 2 min.
(L) Lifetime of each intermediate in ChRmine WT and mutants.

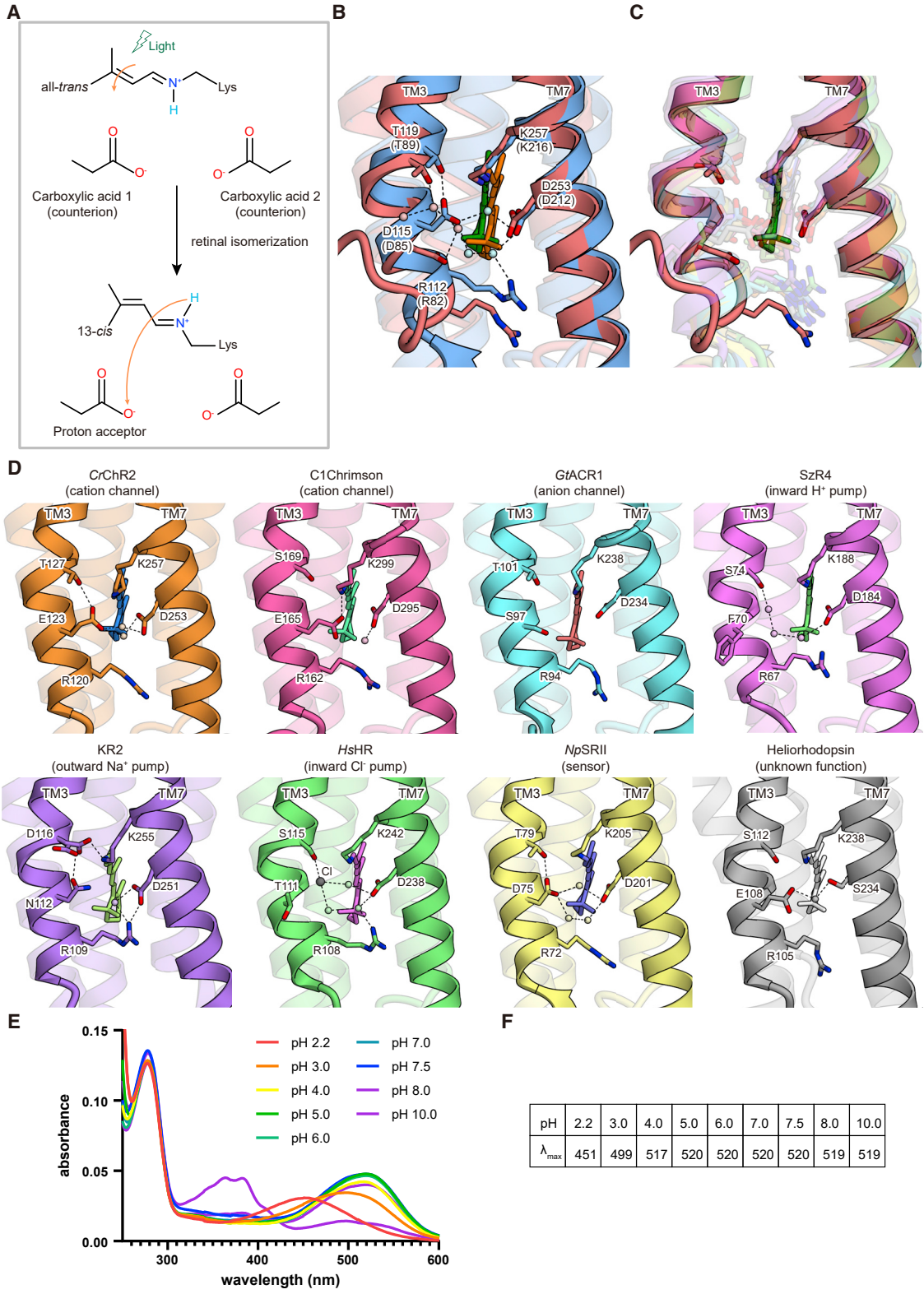

pH	2.2	3.0	4.0	5.0	6.0	7.0	7.5	8.0	10.0
λ_{max}	451	499	517	520	520	520	520	519	519

(legend on next page)

Figure S4. Comparison of the Schiff base regions, related to Figure 2

(A) Concept of the Schiff base counterions and proton acceptor.

(B) The superposed Schiff base region of ChRmine (red) and *Hs*BR (blue). Red and blue spheres represent water molecules of ChRmine and *Hs*BR, respectively. Black dashed lines represent hydrogen bonds.

(C) Superposed Schiff base region of ChRmine (red) and representative microbial rhodopsins (*Cr*ChR2 [Volkov et al., 2017], C1Chrimson [Oda et al., 2018], *Gt*ACR1 [Kim et al., 2018], schizorhodopsin 4 [SzR4] [Higuchi et al., 2021], KR2 [Kato et al., 2015b], *Hs*HR [Kolbe et al., 2000], *Np*SRII [Gordeliy et al., 2002], heliorhodopsin [Shihoya et al., 2019]), displayed with high transparency except for ChRmine.

(D) List of the Schiff base regions of representative microbial rhodopsins.

(E and F) pH titration experiment of WT ChRmine. (E) Absorption spectra of WT ChRmine measured from pH 2.2 to 10.0. (F) The λ_{max} value at each pH.

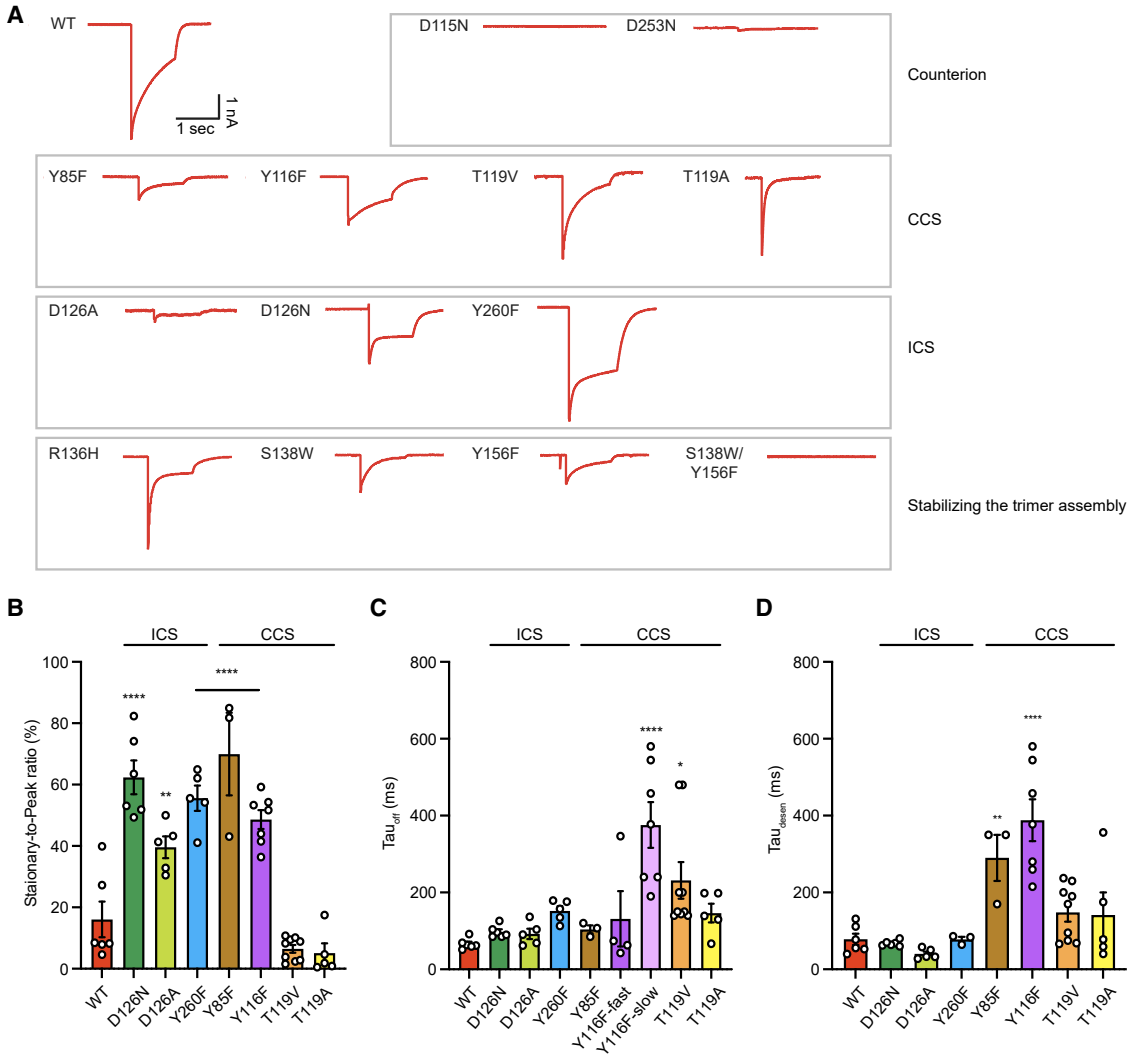

Figure S5. Electrophysiology, related to Figures 2–4

(A) Representative traces of ChRmine WT and 13 mutants expressed in HEK293 cells by lipofectamine transfection, measured at −70 mV holding potential in voltage clamp. Traces were recorded while cells were stimulated with 1.0 s of 1 mW mm^{-2} irradiance at 580 nm.

(B–D) Summary of the steady-to-peak ratio of photocurrents (B), τ_{off} of channel closing (C), and τ_{off} of channel desensitization (=τ_{desen}) (D). Mutants are categorized as the mutants of counterions, central constriction site (CCS), intracellular constriction site (ICS), and the trimer interface. Data are mean ± S.E.M (n = 3–9); one-way ANOVA followed by Dunnett's test. *p < 0.05, **p < 0.01, ***p < 0.001, and ****p < 0.0001.

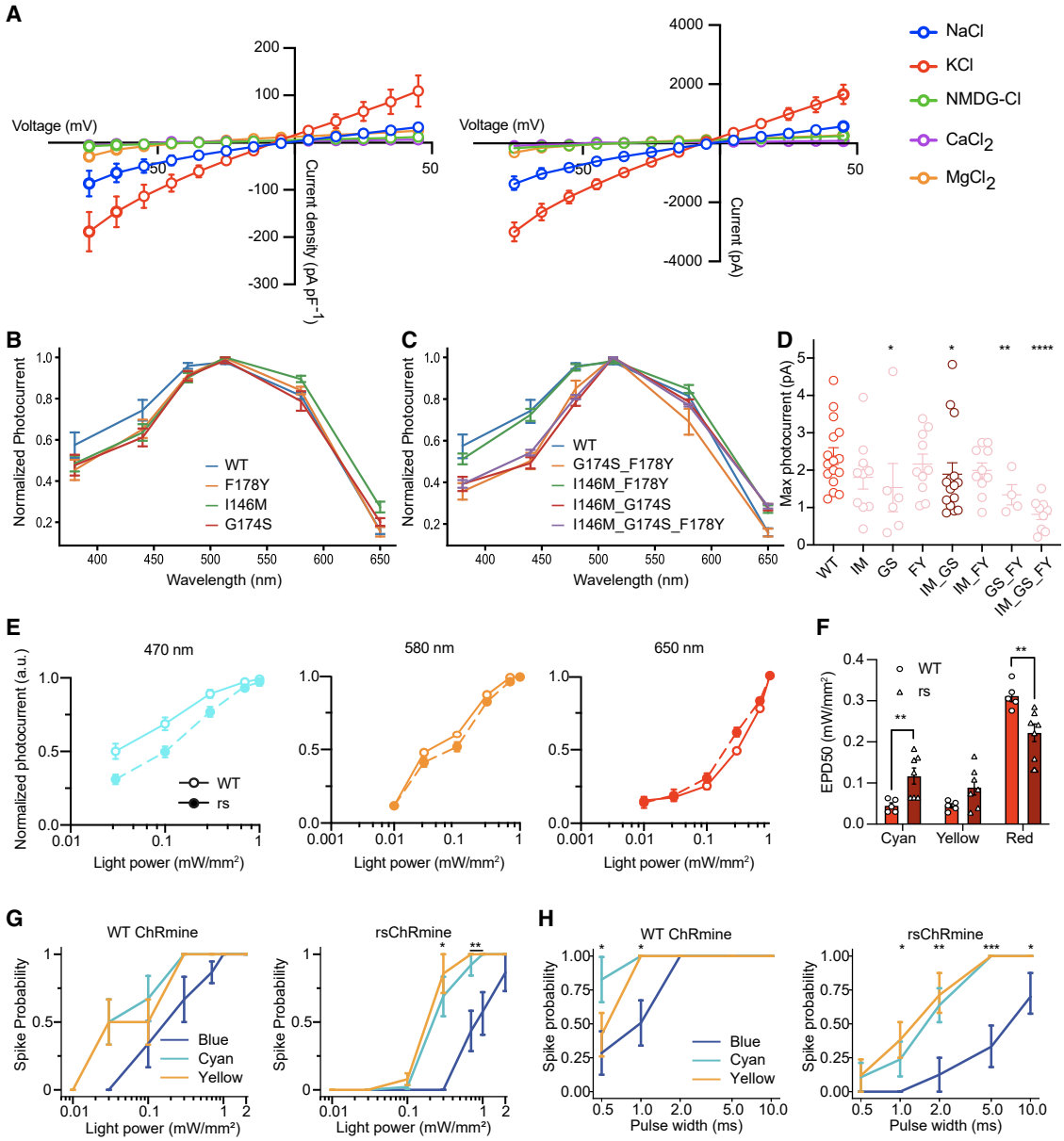

Figure S6. Detailed characterization of rsChRmine, related to Figure 5

(A) The current-voltage dependence of non-normalized (left) and normalized (right) peak photocurrents of ChRmine at different voltages from −75 to 45 mV stimulated with 1 s of 1 mW mm^{-2} irradiance at 580 nm (n = 6–10).

(B and C) Action spectra of single (B), double, and triple (C) mutants of residues in the RBP (n = 4–16).

(D) Peak photocurrents for RBP mutants (n = 4–16, Kruskal-Wallis test with Dunn's test, asterisks denote comparisons with WT ChRmine, *p < 0.05, **p < 0.01, and ****p < 0.0001).

(E) Normalized photocurrent versus light power in cultured neurons with cyan (470 nm), orange (585 nm), and red (650 nm) light (n = 5 for WT and 7 for rs).

(F) Effective power density (EPD50) of WT and rsChRmine (two-tailed Student's t test, n = 5 for WT and 7 for rs, *p < 0.05, **p < 0.01, ***p < 0.001, and ****p < 0.0001).

(G and H) Spike probability versus light intensity (G) and pulse width (H) in cultured neurons expressing opsins (n = 6 for WT and 7 for rs, Kruskal-Wallis test with Dunn's test). All data are mean ± SEM, and sample size n denotes the number of cells unless otherwise noted. *p < 0.05, **p < 0.01, ***p < 0.001, and ****p < 0.0001.

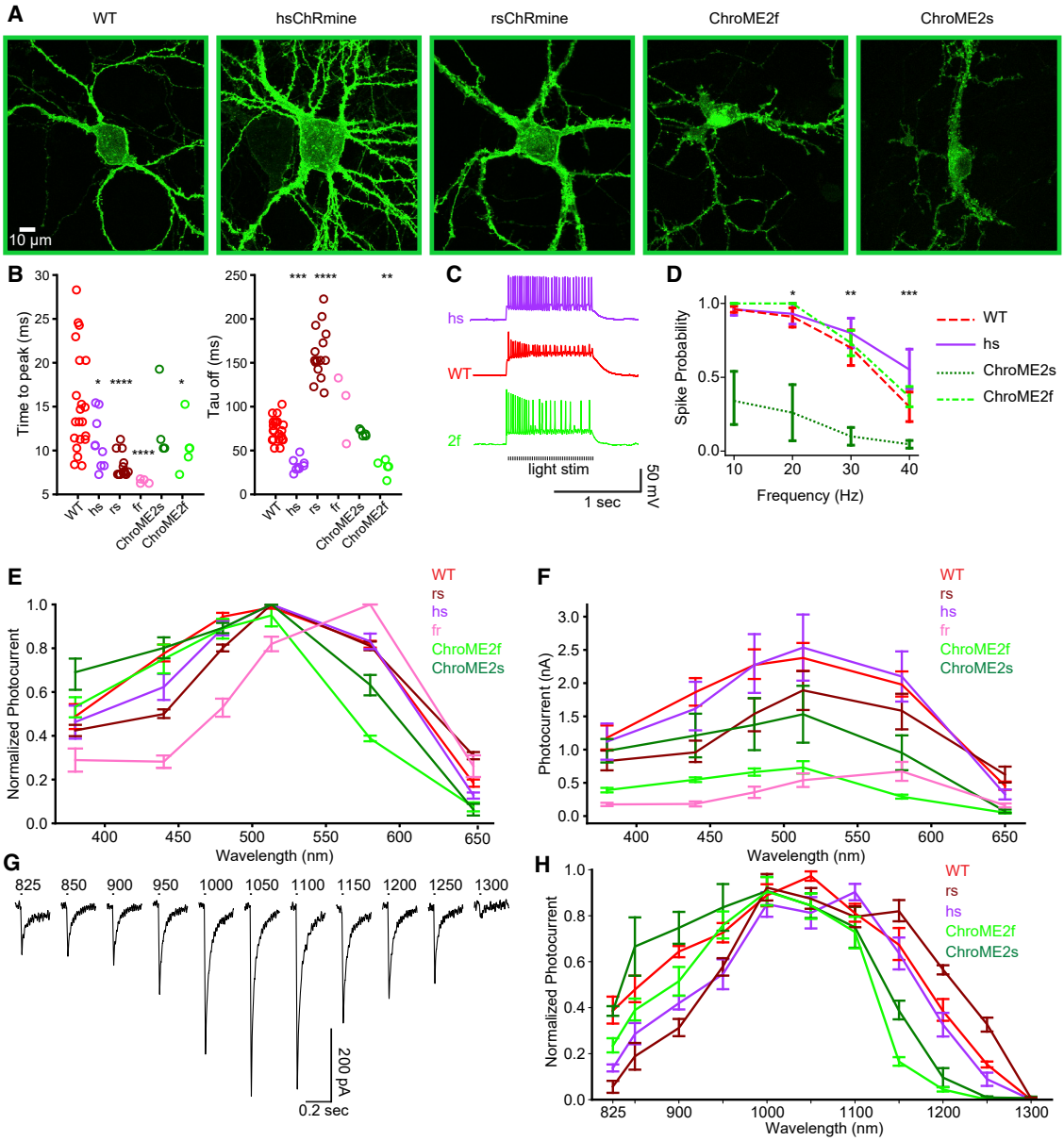

Figure S7. Detailed comparison of ChRmine with ChroME variants, related to Figure 5

(A) Confocal images of WT ChRmine-, hsChRmine-, rsChRmine-, ChroME2f-, and ChroME2s-expressing cultured neurons. Scale bars, 10 µm.

(B) Summary of on (left) and off (right) kinetics of ChRmine and ChroME variants (n = 3–23, Kruskal-Wallis test with Dunn's test. Asterisks denote comparisons with WT ChRmine, *p < 0.05, **p < 0.01, ***p < 0.001, and ****p < 0.0001).

(C) Example current clamp traces of hsChRmine-, WT ChRmine- and ChroME2f-expressing neurons with light stimulation.

(D) Summary of opsin spike fidelity (n = 5 for all mutants, Kruskal-Wallis test with Dunn's test. Asterisks denote comparisons between ChroME2s and WT ChRmine, *p < 0.05, **p < 0.01, and ***p < 0.001).

(E and F) Normalized (E) and peak photocurrent (F) action spectra of ChRmine and ChroME variants (n = 4–16).

(G and H) Example traces of rsChRmine (G) and normalized action spectra (H) of ChRmine and ChroME variants under two-photon excitation (n = 4–6). All data are mean ± SEM, and the sample size n denotes the number of cells unless otherwise noted. For WT ChRmine (compared here under identical conditions alongside other ChRs in the same preparation for rigorous and unbiased comparison of performance regarding photocurrents, action spectra, spike frequency-response, and EPD50), we observed slightly lower spike fidelity than had been observed in Marshel et al. (2019); this can be seen with preparation-to-preparation variance of opsin expression level in cultured neurons.